Modification of the Wilshire strain equation: An application to RR1000

T.A. Williams[a] , M. Evans[b]*, S.J. Williams[c] and S.E. John[d]

[a] Institute of Structural Materials, Swansea University Bay Campus, SA1 8EN, Swansea, Wales, 825982@swansea.ac.uk; [b] College of Engineering, Swansea University Bay Campus, SA1 8EN, Swansea, Wales, m.evans@swansea.ac.uk; [c] Institute of Structural Materials, Swansea University Bay Campus, SA1 8EN, Swansea, Wales; 2031771@swansea.ac.uk; [d] Institute of Structural Materials, Swansea University Bay Campus, SA1 8EN, Swansea, Wales; s.e.john@swansea.ac.uk

*Corresponding author

ABSTRACT

Being able to accurately predict creep strain as a function of time is important both in preventing aeroengine blades rubbing against their outer casings, but also in being able to convert small punch test data into equivalent uniaxial test results using finite element models. Modern studies have found success in applying the Wilshire equations to uniaxial creep test results. The capability of the Wilshire equation to interpolate creep curves was assessed using uniaxial creep tests carried out on RR1000. In this paper, an artificial neural network (ANN) was used to modify the Wilshire equation for the time taken to reach various strains so that the parameters of the Wilshire equation could be interpolated as a function of strain. The model was then evaluated using statistics on predictive accuracy, which showed that the model was capable of predicting the shape and scale of the creep curves with high accuracy. These modifications also revealed that the activation energy is dependent upon the average internal stress and thus strain.

Keywords: Creep Curve; Wilshire Equations; Time to Strains; Forecast Evaluation; artificial neural networks.

Introduction

Uniaxial creep data plays an extremely important role in predicting the life cycle of different alloys used in power generation and aero engines. These engineering applications require materials that can survive the harsh environments of high temperature and stresses [1]. Additionally, a continued rise in energy prices, mounting environmental concerns and growing demand for air travel, require a further increase in the efficiency of the engine through higher operating temperatures [2]. To achieve these higher temperatures, new materials with enhanced creep properties need to be explored and the Nickel based super alloys, such as Waspaloy and RR1000 have shown some promise in this respect. The process from concept to application can be long and expensive due to the test and research programmes that are required to replicate the conditions found in service and the Wilshire equations [3] have been shown to provide reliable extrapolation from short-term measurements made under uniaxial test conditions.

Strain is a very important parameter to consider during design - for example in the aerospace industry it is key to preventing the turbine blades rubbing against the outer casing of the engine. Additionally, being able to realistically predict strain at given times is also very important for converting small punch test loads into equivalent uniaxial stresses - given that the most promising way of doing this is via finite element models of the punch test. These finite element models require equations for working out incremental increases in strain with time and so require accurate predictions of all points along a uniaxial creep curve. The successful correlation of small punch and uniaxial test results will therefore help release the full potential of the small punch test. Recent literature has shown that failure times and minimum creep rates can be predicted reliably from accelerated test data, with scope to further explore the ability to predict time to strains [4-

12]. Evans and Williams [13] have modified the existing Wilshire equations so that entire creep curves can be predicted using accelerated tests at a range of conditions, and analysed the interpolated and/or extrapolated creep curves using modern statistical techniques. Given the importance of strain for developing new aeroengine materials, the aim of this paper is to build on this work by exploring the suitability of this modified Wilshire equation in predicting the times to various strains for the Nickel based super alloy RR1000.

To achieve this aim, the paper is structured in the following way. The next section describes the creep test matrix used and some additional material characteristics and properties of RR1000, and the normalisation procedures used to protect the commercial sensitivity of this data to its developers. This is followed by sections looking at the Wilshire equations as applied to the time to failure and times to various strains and the criteria used to assess how good the Wilshire equations are at predicting creep curves for RR1000. The final section concludes by discussing pathways for possible future research.

Test Matrix, Material Characteristics and Material Properties

RR1000 is a powder processed γ′ precipitation strengthened nickel-base superalloy produced by Rolls-Royce whose chemical composition is given in Table 1. This chemical composition (in wt%) is very similar to that found by Mitchell *et. al*. [14], who also provide detailed description of the manufacture, heat treatment and microstructural evolution of RR1000.

Table 1. Composition of RR1000 in Weight Percent.

As part of a funded research program, Rolls-Royce supplied results from uniaxial creep tests carried out on thirty five test piece specimens which were machined from fine grained RR1000 bars with the above chemical composition and heat treatment as described by Mitchell *et. al*. [14]. The specimens were creep strain tested in an air environment on constant-stress creep machines at the Rolls-Royce Derby site test labs. These specimens were tested at six different temperatures, 848 K, 873 K, 898 K, 923 K, 948 K and 998 K, and at each temperature a range of different stresses were used. At 848K a specimen was tested at 1410 MPa and 1370MPa. At 873K, six specimens were used to test at stresses ranging from 1300 MPa to 1000 MPa. At 898K, five specimens were used to test at stresses ranging from 1190 MPa to 900 MPa. At 923K, twelve specimens were used to test at stresses ranging from 1190 MPa to 700 MPa. At 948K, four specimens were used to test at stresses ranging from 1005 MPa to 591 MPa and at 998K six specimens were used to test at stresses ranging from 1005 MPa to 263 MPa. The tensile strength (σ_{TS}) of the RR1000 material from which these test specimens were cut were measured at 1504 MPa, 1495 MPa, 1472 MPa, 1448 MPa, 1373 MPa and 1210 MPa at 848 K, 873 K, 898 K, 923 K, 948 K and 998K respectively.

Figures 1(a,b) below consist of micrographs of the chemically etched fine grained RR1000 material used in this paper. As a consequence of etching, the γ phase has been removed leaving just the trimodal distribution of gamma primes, γ'. Large darker primary gamma prime precipitates with sizes ranging from between 0.5-3μm are observed. These tend to form during the forging process and act to strengthen against creep strain through the pinning of the grain boundaries, providing creep strain resistance at higher temperature through the hindering of dislocations as a result of bowing. Due to this pinning of the grain boundaries, grain growth is restricted and thus provides the fine

equiaxed structure also observed by Mitchel *et. al.* [15]. Smaller, secondary (200nm) and tertiary (~15nm) gamma primes also exist within the γ grains providing good intergranular precipitation strengthening effects [16].

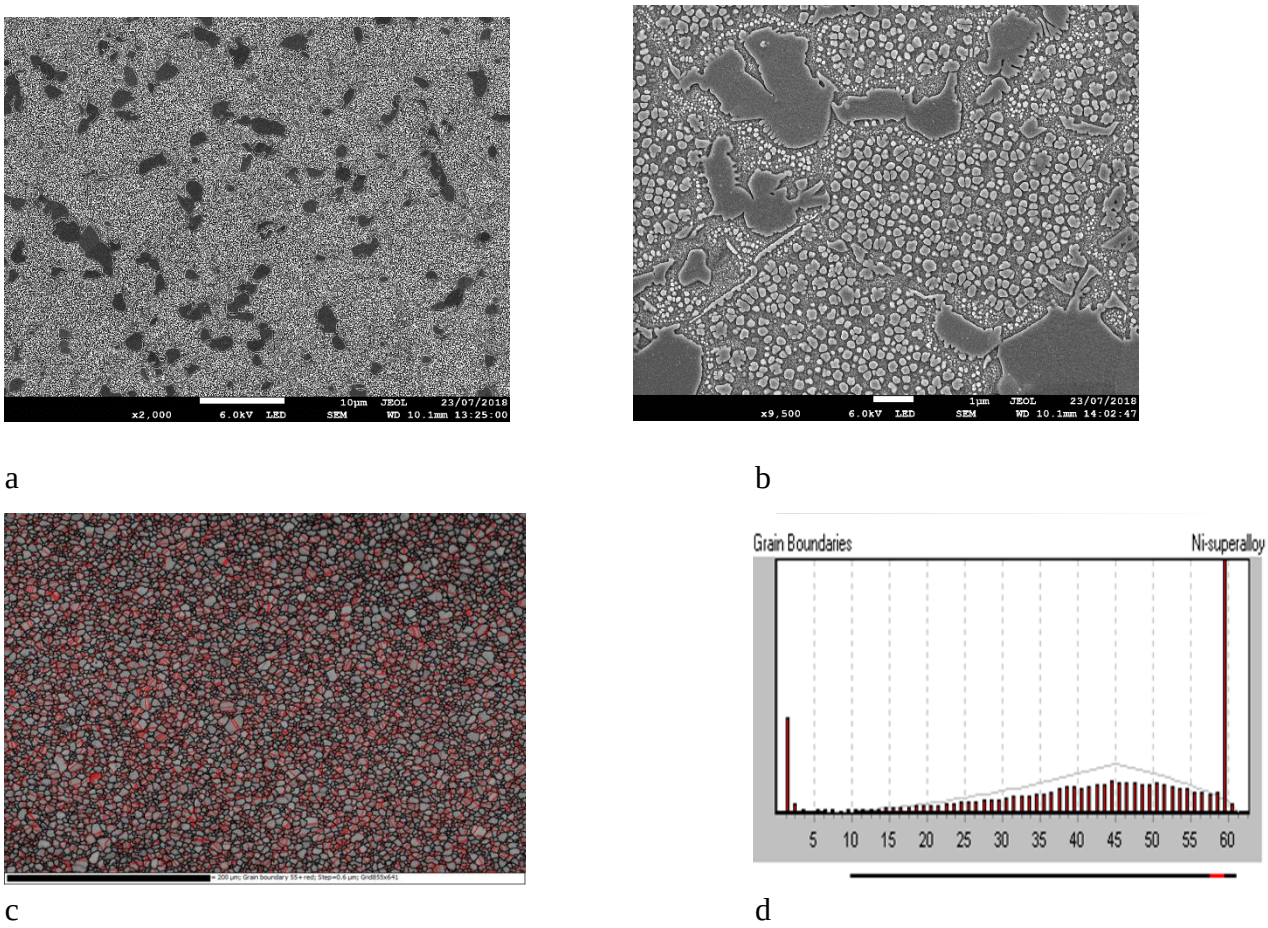

a b

c d

Figure 1. (a,b) Micrographs of the chemically etched fine grained RR1000, (c,d) EBSD maps showing grain boundary types.

In polycrystalline Nickel based superalloys used for high temperature applications, grain boundaries can be engineered to improve fatigue, creep and corrosion resistance. This is completed through the addition of coincident site lattices (CSL). The degree of misorientation and thus coherency of a grain boundary is defined as a CSL,

which has a subsequent Σ value. Low angle CSL boundaries (Σ > 29) contain large defects, and thus promote creep diffusion mechanisms. However, high CSL values (Σ < 29) are coherent and contain less defects and are therefore ideal for materials subjected to high temperatures. Twins are a common example of a high CSL boundary used for creep strengthening, and occur at a misorientation angle of 60 ± 5 (Σ = 3) [17]. Figures 1(c,d) provide an EBSD map showing the grain boundary types that exist within the unetched fine grained RR1000 used in this paper. Figure 1(c) shows a peak at ~60^{o} (twin boundaries) with these boundaries highlighted in red, and these make up 21.7% of all boundaries present. This suggests the composition of RR1000 will have superior creep properties at elevated temperature.

RR1000 is a commercially sensitive material to Rolls-Royce and so to protect these interests some of the data used in this paper has been normalised in the following ways:

$$\varepsilon_n = \varepsilon/\varepsilon_f \tag{1a}$$

where ε is the strain experienced by a specimen on test, ε_f the specimens strain at failure and ε_n the normalised strain at failure. For failure times t_f, normalisation is done with respect to the log transformed failure time

$$\ln[t_{fn}] = \frac{\ln[t_f]-\ln[t_f]_{min}}{\ln[t_f]_{max}-\ln[t_f]_{min}} \tag{1b}$$

where $\ln[t_f]_{min}$ is the minimum log failure time obtained over all the above mentioned test conditions and $\ln[t_f]_{max}$ the corresponding maximum value.

Finally, the time taken to reach a specified normalised strain, $t_{\varepsilon n}$, is also normalised with respect to the log transformation of these times,

$$\ln[t_{n\varepsilon n}] = \frac{\ln[t_{\varepsilon n}] - \ln[t_{\varepsilon n}]_{min}}{\ln[t_{\varepsilon n}]_{max} - \ln[t_{\varepsilon n}]_{min}} \quad (1c)$$

where $\ln[t_{\varepsilon n}]_{min}$ is the minimum, over all the above mentioned test conditions, of the logged times to reach a normalised strain of ε_n and $\ln[t_{\varepsilon n}]_{max}$ the maximum value. The maximum and minimum failure times, times to various normalised strains and the rupture strains in this data set are not disclosed in this paper to protect the identity of the actual failure and strain times (and nor is the unit of time to which the log transformations are applied).

Thus $t_{n\varepsilon n}$ and t_{fn} are linear scaled variables that take on values within the limits zero to one and so this transformation does not alter the underlying relationships between time, stress and temperature. Knowing the maximum and minimum values is enough to rescale the Wilshire models parameters shown in this paper to obtain the true values for strain and time.

The Wilshire equations

Wilshire postulated three equations to describe the stress and temperature dependencies of the minimum creep rate, times to failure and times to given strain. This paper will concentrate on the time to failure and times to strain equations.

Time to failure

The Wilshire equation for the minimum creep rate ($\dot{\varepsilon}_m$) acts as the fundamental link from which all the other Wilshire equations can be derived. The Wilshire equation for the minimum creep rate takes the form

$$\sigma/\sigma_{TS} = \exp\left\{-k_{2j}\left[\dot{\varepsilon}_m \exp\left(Q^*_{cj}/RT\right)\right]^{v_j}\right\} \qquad \text{for } j = 1 \text{ to } p \tag{2a}$$

and using the Monkman-Grant relation [18] with an exponent equal to unity, this can be converted into an equation for time to failure t_f that is given by

$$\sigma/\sigma_{TS} = \exp\left\{-k_{1j}\left[t_f \exp\left(-Q^*_{cj}/RT\right)\right]^{u_j}\right\} \quad \text{for} \quad j = 1 \text{ to } p \tag{2b}$$

$j = 1$ when $\sigma/\sigma_{TS} \le \sigma_1^c$; $j = 2$ when $\sigma_1^c < \sigma/\sigma_{TS} \le \sigma_2^c$; …. ; $j = p$ when $\sigma/\sigma_{TS} > \sigma^c_{p-1}$

$$\sigma_1^c < \sigma_2^c < \ldots\ldots\ldots < \sigma^c_{p-1}$$

where T is the absolute temperature (K), σ the stress (MPa), σ_{TS} the tensile strength (MPa), R the universal gas constant and Q^*_{cj} are the activation energies in each of the p normalised stress ranges. k_{1j} ,k_{2j}, u_j and v_j are parameters that require estimation (as do the activation energies). σ^c_j are critical values for the normalised stress and so fall between 0 and 1. In this approach, there are p creep regimes that occur in distinct ranges for the normalised stress and the p versions of equation [2b] then apply to each regime. Typically, p varies between 1 and 4 depending on the material being studied. One issue with the Wilshire equations, that has to some extent limited its adoption in industry, is that it is not based on any particular creep theory, or even on any Continuum damage mechanism specification. Whilst the temperature expression is loosely based on a an Arrhenius type relation, the stress transformation has no theoretical basis, other than t_f tends to infinity in a sigmoidal fashion as the normalised stress tend to zero (and t_f tends to zero as the

stress approach the materials tensile strength). Whilst this makes intuitive sense, there are many other stress transformations that have this property.

Another limitation of this (and the other) Wilshire equation is that the value for p is not known and so this must be determined from the experimental data, with additional investigation then required to determine or explain the different creep mechanisms accounting for each of the p regimes. An example of this is given in the application section below. Whilst increasing p will tend to produce better fits to short term data, it is likely to results in poor extrapolations of safe life determination.

Equation [2b] can also be written as:

$$\ln[t_f] = a_{0j} + a_{1j}\ln[-\ln(\sigma/\sigma_{TS})] + a_{2j}[1/RT] \; ; \qquad j = 1 \text{ to } p \qquad (2c)$$

where $u_j = 1/a_{1j}$, $k_{1j} = \exp(-a_{0j}/a_{1j})$ and $Q^*_{cj} = a_{2j}$. Replacing $\ln[t_f]$ in equation [2c] with $\ln[t_{fn}]$ in equation [1b] yields

$$\ln[t_{fn}] = b_{0j} + b_{1j}\ln[-\ln(\sigma/\sigma_{TS})] + b_{2j}[1/RT] \; ; \qquad j = 1 \text{ to } p \qquad (2d)$$

and the link between equation [2c] and equation [2d] is given by $a_{0j} = \ln[t_f]_{min} + b_{0j}\{\ln[t_f]_{max} - \ln[t_f]_{min}\}$, $a_{1j} = b_{1j}\{\ln[t_f]_{max} - \ln[t_f]_{min}\}$ and $a_{2j} = b_{2j}\{\ln[t_f]_{max} - \ln[t_f]_{min}\}$. Thus obtaining estimates for all the b parameters in equation [2c] allows values for the original Wilshire parameters (u, k_1 and Q^*_c) to be quantified provided the minimum and maximum failure times in the data set used for such estimation are known.

When p = 1 the parameters b_{01} to b_{21} are estimated using the least squares technique through the regression of $\ln[t_{fn}]$ on $\ln[-\ln(\sigma/\sigma_{TS})]$ and 1/RT. But when p = 2,

two new variables are created using the value for σ^c_1:

$$\ln[t_{fn}] = b_0 + b_1\ln[-\ln(\sigma/\sigma_{TS})]+b_2\,[1/RT] + b_3 Max(0, \sigma^*)+b_4\,[D/RT] \quad (2e)$$

where $\sigma^* = \ln[-\ln(\sigma/\sigma_{TS})] - \ln[-\ln(\sigma^c_1)]$, D = 0 when $\sigma^* \leq 0$ and D = 1 when $\sigma^* > 0$. When j = 1 and so $\sigma^* \leq 0$, equation [2e] collapses to

$$\ln[t_f n] = b_0 + b_1\ln[-\ln(\sigma/\sigma_{TS})]+b_2\,[1/RT]$$

and so $b_{01} = b_0$, $b_{11} = b_1$ and $b_{21} = b_2$. Thus $u_1 = 1/(b_1\{\ln[t_f]_{max} - \ln[t_f]_{min}\})$ and $Q^*_{c1} = b_2\{\ln[t_f]_{max} - \ln[t_f]_{min}\}$. Then when j = 2 and so $\sigma^* > 0$ with D = 1, equation [2] can be re-arranged as

$$\ln[t_{fn}] = \{b_0 - b_3\ln[-\ln(\sigma^*)]\} + (b_1 + b_3)\ln[-\ln(\sigma/\sigma_{TS})]+ (b_2 + b_4)\,[1/RT] \quad (2f)$$

and so $b_{02} = b_0 - b_3\ln[-\ln(\sigma^*)]$, $b_{12} = b_1 + b_3$ and $b_{22} = b_2 + b_4$. Thus $u_2 = 1/(b_{12}\{\ln[t_f]_{max} - \ln[t_f]_{min}\})$ and $Q^*_{c2} = b_{22}\{\ln[t_f]_{max} - \ln[t_f]_{min}\}$. All these parameters are estimated by a regression of $\ln[t_{fn}]$ on $\ln[-\ln(\sigma/\sigma_{TS})]$, 1/RT, $Max(0, \sigma^*)$ and D/RT. This regression will have an associated coefficient of determination (R^2) - that shows what percentage of the variation in $\ln[t_{fn}]$ that can be explained by variations in all the variables on the right hand side of equation [2e]. This regression is carried out for all values of σ^c_1 within the experimental range of normalised stresses and the value σ^c_1 is that value which gives the largest R^2 value.

Time to specified strains

Equation [2b] simply explains how the time at the end point of a creep curve varies with the stress and temperature used to obtain that curve. But in principle a comparison can be made using any time point on a creep curve, provided it is the same point, i.e. the time to the same specified strain ε. This idea is what lies behind the Wilshire equation for times to a given strain, which as originally specified takes the form:

$$\sigma/\sigma_{TS} = \exp\left\{-k_{3j}\left[t_{\varepsilon}\exp\left(-Q^{*}_{cj}/RT\right)\right]^{w_j}\right\} \quad ; \quad j = 1 \text{ to } p \qquad (3a)$$

where t_ε is time to reach the strain value of ε. k_{3j} and w_j are once again parameters that require estimation. However, this equation cannot be a true description of this relationship because the strain at failure is in part temperature and stress dependant, with rupture strain tending to be smaller at lower stresses. This implies equation [3a] does not hold for all values of the normalised stress, with the relationship being truncated at some critical normalised stress and temperature. Consequently, at certain normalised stresses and temperatures some specimens within the test data set described above will already have succumbed to failure and therefore no t_ε value will be available. Therefore equation [3a] should really be written in terms of times to given normalised strains, because then no matter what the test condition is for a creep specimen, it will always have a normalised strain, (and therefore a time to that strain), varying over the full range from $\varepsilon_n = 0$ to $\varepsilon_n = 1$

$$\sigma/\sigma_{TS} = \exp\left\{-k_{4j}\left[t_{\varepsilon n}\exp\left(-Q^{*}_{cj}/RT\right)\right]^{z_j}\right\} \quad ; \quad j = 1 \text{ to } p \qquad (3b)$$

which can be expressed as

$$\ln[t_{\varepsilon n}] = c_{0j} + c_{1j}\ln[-\ln(\sigma/\sigma_{TS})] + c_{2j}[1/RT] \quad ; \quad j = 1 \text{ to } p \qquad (3c)$$

where $z_j = 1/c_{1j}$, $k_{4j} = \exp(-c_{0j}/c_{1j})$ and $Q_{cj}^{*} = c_{2j}$. Replacing $\ln[t_{\varepsilon n}]$ in equation [3c] with

its normalised equivalent as given byequation [1c] yields

$$\ln[t_{n\varepsilon n}] = d_{0j} + d_{1j}\ln[-\ln(\sigma/\sigma_{TS})] + d_{2j}[1/RT] \;; \qquad j = 1 \text{ to } p \tag{3d}$$

and the link between equation [3c] and equation [3d] is given by $c_{0j} = \ln[t_{n\varepsilon n}]_{min} + d_{0j}\{\ln[t_{n\varepsilon n}]_{max} - \ln[t_{n\varepsilon n}]_{min}\}$, $c_{1j} = d_{1j}\{\ln[t_{n\varepsilon n}]_{max} - \ln[t_{n\varepsilon n}]_{min}\}$, and $c_{2j} = d_{2j}\{\ln[t_{n\varepsilon n}]_{max} - \ln[t_{n\varepsilon n}]_{min}\}$. Thus obtaining estimates for all the d parameters in equation [3d] allows values for the Wilshire parameters (z, k_4 and Q^*_c) to be quantified - provided the minimum and maximum times to a specified normalised strain in the data set used for such estimation are known.

Again the values for parameters of d_{0j} to d_{2j} can be estimated using the least squares method through the regression of $\ln[t_{n\varepsilon n}]$ on $\ln[-\ln(\sigma/\sigma_{TS})]$ and 1/RT. Once again, a break can be allowed for by using the dummy variable D as defined above

$$\ln[t_{n\varepsilon n}] = d_0 + d_1\ln[-\ln(\sigma/\sigma_{TS})] + d_2[1/RT] + d_3 Max(0, \sigma^*) + d_4[D/RT] \tag{3e}$$

For equations (2b,3b) to be consistent, $k_{4j} \rightarrow k_{1j}$ and $z_j \rightarrow u_j$ as ε_n tends towards unity. These Wilshire parameters will be functions of strain, whose exact form is unknown. These unknown functions are expressed as f_{1j} and f_{2j} in equation [3f]

$$z_j = f_{1j}(\varepsilon_n) \quad \text{and} \quad k_{4j} = f_{2j}(\varepsilon_n) \tag{3f}$$

It follows from equations [3b,3f] that a normalised uniaxial creep curve at any test condition is given by:

$$t_{\varepsilon n} = -\frac{[\ln(\sigma/\sigma_{TS})/f_{2j}(\varepsilon_n)]^{1/f_{1j}(\varepsilon_n)}}{\exp\left(-Q^*_{cj}/RT\right)} \tag{3g}$$

Further this normalised time can be converted into actual time using equation [1c] provided the maximum and minimum times to specified strains are known.

Modelling $f_{1j}(\varepsilon_n)$ and $f_{2j}(\varepsilon_n)$

For equation [3g] to be used for predictive purposes, expressions for f_{1j} and f_{2j} are required but these are currently unknown. These nature of these relationships have not as yet been extensively researched. The few exceptions include a study by Abdallah et. al. [18] who assumed the w_{3j} in equation [3a] were fixed with respect to strain when studying Titanium (but strangely did not specify a form for $f_{2j}(\varepsilon)$). Harrison et. al. [19], when studying Nickel based super alloys, again assumed w_{3j} to be fixed but with $k_{3j} = k_{3j,0}+k_{3j,1}\varepsilon^{-k_{3j,2}}$. The problem with this specification is that it does not ensure $k_{3j} \rightarrow k_{1j}$ as $\varepsilon \rightarrow \varepsilon_f$. More recently, Gray and Whittaker [20] when studying Waspaloy proposed a model for predicted creep curves that appeared to bypass the Wilshire methodology altogether by working with

$$t_\varepsilon = M(\varepsilon)\frac{\left(1 - \frac{\sigma}{\sigma_{TS}}\right)^{P(\varepsilon)}}{\exp\left(-Q_c^{***}/RT\right)}$$

where M and P are parameters whose value depends in some way of the strain ε. The authors also observed a complicated relationship between P and ε and also between M and ε which they modelled using

$$M(\varepsilon) = A_1\exp\left(-\left(\varepsilon/A_2\right)^{-A_3}\right) \quad ; \qquad P(\varepsilon) = A_7 + \frac{A_4}{\varepsilon A_5\sqrt{2\pi}}\exp\left(-\ln\left(\frac{A_6\varepsilon}{2A_5^2}\right)^2\right)$$

where A_1 to A_7 are model parameters that require estimation – the model is not particularly parsimonious therefore. These parameters are not consistent with the

298 Wilshire time to failure equation in that there is not guarantee that as ε tends to the rupture
299 strain, these equations will produce values for k_{3j} and w_j that tend to k_{1j} and u_j. As result
300 it is possible for these equation to predict creep curve shapes that double back on
301 themselves at high strains.

302 For these reasons this paper adopts a different approach. The approach is entirely
303 empirical in nature, and so one of its limitations is that no physically meaningful
304 interpretation can be given to its parameters. But it does have the advantage that k_{3j} and
305 w_j tend to k_{1j} and u_j as strain approach the rupture strain (and so avoids the issue of
306 doubling back). It is also much simpler to estimate the parameters of this empirical model
307 as it only requires simple linear optimisation procedures – such as linear least squares.
308 The empirical approach adopted for this paper is an Artificial Neural Network (ANN)
309 which is used to represent the functional forms in Eq. (3e), so that the Wilshire approach
310 in Eq. (3f) can then be used to model the creep curve. Following Martin et. al. [21] this
311 ANN is specified as

312 $$d_{1j} = \phi_{0j} + \phi_{1j}\varepsilon_n + \sum_{i=1}^{m} \beta_{ij} \left[\frac{1}{1+\exp(\delta_{0ij}+\delta_{1ij}\varepsilon_n)}\right] \qquad j = 1 \text{ to } p \qquad (4a)$$

313 $$d_{0j} = \phi_{2j} + \phi_{3j}\varepsilon_n + \sum_{i=1}^{m} \lambda_{ij} \left[\frac{1}{1+\exp(\delta_{2ij}+\delta_{3ij}\varepsilon_n)}\right] \qquad j = 1 \text{ to } p \qquad (4b)$$

314

315 with these predicted values for d_{0j} and d_{1j} being easily convertible to values for the
316 original Wilshire parameters z_j and k_{4j} in the ways described earlier.

317 It is also possible that the Q^*_{cj} varies with the normalised strain. For example,
318 Davies [22] first suggested that the activation energy is only constant during steady state
319 creep where a dynamic equilibrium rate occurs. Outside steady state creep he proposed

that the activation energy would be dependent upon the average internal stress. Further, Estrin and Mecking [23] showed that the evolution of the internal stress can be derived from the evolution of the dislocation density as a function of the creep strain (via a first order partial differential equation)) so that the activation is also a function of strain. More precisely they showed that the activation energy is a modified exponentially function of strain such that as strain increases the activation energy tends to that associated with steady state creep. To allow for this type of variation, Q^*_{cj} can also be given an ANN representation

$$Q^*_{cj} = \phi_{4j} + \phi_{5j}\varepsilon_n + \sum_{i=1}^{m} \gamma_{ij} \left[\frac{1}{1+\exp(\delta_{4ij}+\delta_{5ij}\varepsilon_n)}\right] \qquad j = 1 \text{ to } p \qquad (4c)$$

If the parameters $\beta_{ij} = \lambda_{ij} = \gamma_{ij} = 0$, then essentially these Wilshire parameters become simple linear functions of the normalised strain. To estimate the unknown parameters of these ANN's, m is first fixed at unity, and values for all the δ parameters are guessed at enabling the expressions in square parenthesis in equations [4] to be converted into numerical variables. For equation [4a] a regression of d_{1j} on ε_n and $\frac{1}{1+\exp(\delta_{0i1}+\delta_{1i1}\varepsilon_n)}$ can then be carried out. This regression will have an associated coefficient of determination - (R^2). This regression is carried out for values of δ_{011} and δ_{111} within a defined 2x2 grid of values for δ_{011} and δ_{111} and the values δ_{011} and δ_{111} are taken to be those values which gives the largest R^2 value.

Another issue associated with ANN's is that a better fit can always be obtained by increasing the value for m in equations [4]. This can result in overfitting, which then usually results in good interpolative capability but very poor extrapolative capability. This is not so much on an issue here, as the purpose of the ANN's in simply to interpolate

between values for the normalised strain over the range 0 – 1. However, to minimise the possibility of over fitting or ensuring the derivation of the most parsimonious model, m can be gradually increased and the following Akaike Information Criteria [24] then used to choose the value for m

$$AIC = S[1-R^2_{max}]\exp[2(3m+2)/n] \quad (5)$$

where n is the number of test specimens and S is the standard deviation in d_{1j} (or d_{0j} when using equation [4b]).

Equation [3g] used in conjunction with equations (4) is enough for the prediction of a full creep curve within the range of experimental test conditions because the value for ε_f is known and can be used to convert ε_n to ε. When predicting the actual creep curves at conditions that lie outside of the experimental test range, the value of ε_f will not be known. One solution to this is to estimate the Monkman - Grant [25] parameters C and ρ as postulated by Dunand *et al.* [26],

$$[\dot{\varepsilon}_m]^{\rho} = C[\varepsilon_f/t_f] \quad (6)$$

and substitute into this relation the predictions for t_f and $\dot{\varepsilon}_m$ given by the above Wilshire equations. This then enables a prediction of the failure strain to be made. This ANN approach is general enough to be universally applicable to all high temperature metals, but so fat has only been applied to the Nickel based superalloy – Waspaloy [13].

Evaluation

The mean squared prediction error (MSPE) is often a good starting point for the evaluation of any predictions made from a particular creep property using a specific model. Letting y^a_i be the experimental (or actual) value for a creep property obtained at

365 the ith test condition (such as at σ = 700 MPa and T = 973K) – e.g. the actual (not
366 normalised) time to failure. If y^p_i is the prediction made for that creep property, then the
367 MSPE (mean square prediction error) is given by

368 $$\text{MSPE} = \frac{\sum_{i=1}^{n}(y_i^a - y_i^p)^2}{n} \quad (7a)$$

369 where there are n creep specimens tested at n different test conditions. Whilst the
370 squaring of the prediction errors prevent under predictions being offset by over
371 predictions in the averaging procedure, the MSPE provides no sense of scale for the
372 prediction errors. One simple modification to equation [7a] that introduces a sense of
373 scale is to replace y^a and y^p with the natural log of their values. This scaling comes about
374 because when using the natural logs of the creep properties and their predictions, the
375 MSPE associated with the logged data is approximately equal to the mean percentage
376 square error (MPSE) associated with the raw (untransformed) data:

377 $$\frac{\sum_{i=1}^{n}(x_i^a - x_i^p)^2}{n} \cong \text{MPSE} = \frac{\sum_{i=1}^{n}([y_i^a - y_i^p]/y_i^p)^2}{n} \quad (7b)$$

378 with this approximation being better the smaller are the percentage errors. In equation
379 [7b], $x^a_i = \ln(y^a_i)$ and $x^p_i = \ln(y^p_i)$.

380 Peel *et. al.* [27] decomposed this MPSE into three separate components using a
381 plot of the actual (but in logs) creep property series against a series made up of the models
382 predictions, namely:

383 $$x_i^a = \alpha_0 + \alpha_1 x_i^p + e_i \quad (8a)$$

where the variable e_i picks up any random scatter around the best fit line on this plot. It follows from this equation that the percentage prediction error is (approximately) given by

$$x_i^a - x_i^p = \alpha_0 + (\alpha_1 - 1)x_i^p + e_i \quad (8b)$$

and so

$$\mathrm{Var}(x_i^a - x_i^p) = (\alpha_1 - 1)^2(\sigma^p)^2 + \sigma_e^2 \quad (8c)$$

where Var() reads the variance of the variable in the brackets, σ^2_e is the variance of the residual term e_i and $(\sigma^p)^2$ is the variance of the variable x^p. The least squares estimate of α_0 is also given by $\overline{x^a} - \alpha_1\overline{x^p}$, where the bar signifies the mean of the variable. Thus $(\overline{x^a} - \overline{x^p})^2 = (\alpha_0 + (\alpha_1 - 1)\overline{x^p})^2$ allowing the MPSE to be decomposed as

$$\mathrm{MPSE} = (\alpha_0 + (\alpha_1 - 1)\overline{x^p})^2 + (\alpha_1 - 1)^2(\sigma^p)^2 + \sigma_e^2 \quad (8d)$$

Therefore, part of the MPSE is attributable to the intercept (α_0) of the best fit line on a plot of x^a_i against x^b_i being different from zero and another part of the MPSE is attributable to slope (α_1) of the best fit line on a plot of x^a_i against x^b_i being different from 1. These parts of the MPSE are systematic in nature as they are caused by this best fit line being different from a 45 degree line on such a plot and so leads to either persistent under or over prediction of the x^a series. The remaining part of the MPSE is a random prediction error whose size is given by the variance of e or the extent to which the data are scattered around the best fit line on a plot of x^a_i against x^b_i. Dividing both sides by the MPSE

$$1 = \frac{(\alpha_0 + (\alpha_1 - 1)\overline{x^p})^2}{\mathrm{MPSE}} + \frac{(\alpha_1 - 1)^2(\sigma^p)^2}{\mathrm{MPSE}} + \frac{\sigma_e^2}{\mathrm{MPSE}} = U^M + U^R + U^D \quad (8e)$$

To make it easier to compare the accuracy of various creep models, the MPSE can also be re-scaled to be within the range zero to one as suggested by Theil [28]

$$U = \frac{\sqrt{\frac{\sum_{i=1}^{n}\left(x_i^a - x_i^p\right)^2}{n}}}{\sqrt{\frac{1}{n}\sum_{i=1}^{n}\left(x_i^a\right)^2} + \sqrt{\frac{1}{n}\sum_{i=1}^{n}\left(x_i^p\right)^2}} \qquad (8f)$$

The numerator of U is the square root of the MPSE and is often called the root mean percentage square error or RMPSE. The denominator scales U to fall between 0 and 1. If U = 0, then $x^a_i = x^b_i$ for all i (i.e. over all the different test conditions) and the model is a perfect predictor of the creep properties under analysis. If U = 1, the predictive performance of the creep model is as bad as it could possibly be. Hence U measures the RMPSE in relative terms.

Application to RR1000 data

The time to failure

Using the method of estimation given above, Table 2a shows the parameter estimates of equation [2d]. The values for b_{21} and b_{22} are not shown in Table 2a. Instead, the activation energies that these parameter values imply are shown instead. (It is not possible to show both these quantities as it would then be possible to rescale the normalised failure times to the true failure times values - within the margins of the experimental scatter). It is felt by the authors that the values for the activation energies are more informative than the values for b_{21} and b_{22}.

Table 2a. Least squares estimates of the parameters of equation [2d].

The parameter b_4 in equation [2e] produced a p-value of 0.577% meaning that the activation energies (Q_c^*) above and below the normalised stress break point of 0.731 ($= \sigma_1^c$) are significantly different from one another at a significance level of 1%. Below the normalised stress of 0.731 the value of Q_c^* is approximately 247 kJ mol^{-1} and above it has a value of 237 kJ mol^{-1}.

The p-value that is associated with b_3 in equation [2e] is 0.479% suggesting that the values for u above and below a normalised stress of 0.731 are significantly different from each other at the 1% significance level. The coefficient of determination, R^2, shows that the model is capable of explaining 92.97% of the variation observed in the logarithm of the times to failure.

A visual representation of this Wilshire relationship can be seen in Figure 2(a), where on the horizontal axis the normalised failure times values are temperature compensated. The good performance of the Wilshire equation is seen by the suitability of the best fit line that is kinked at the break point defined by a normalised stress of 0.731. Alternatively, in Figure 2(b), σ/σ_{TS} is plotted against the actual and the models predicted normalised times to failure. The predictions shown by the solid lines give a good fit to the actual normalised failure times.

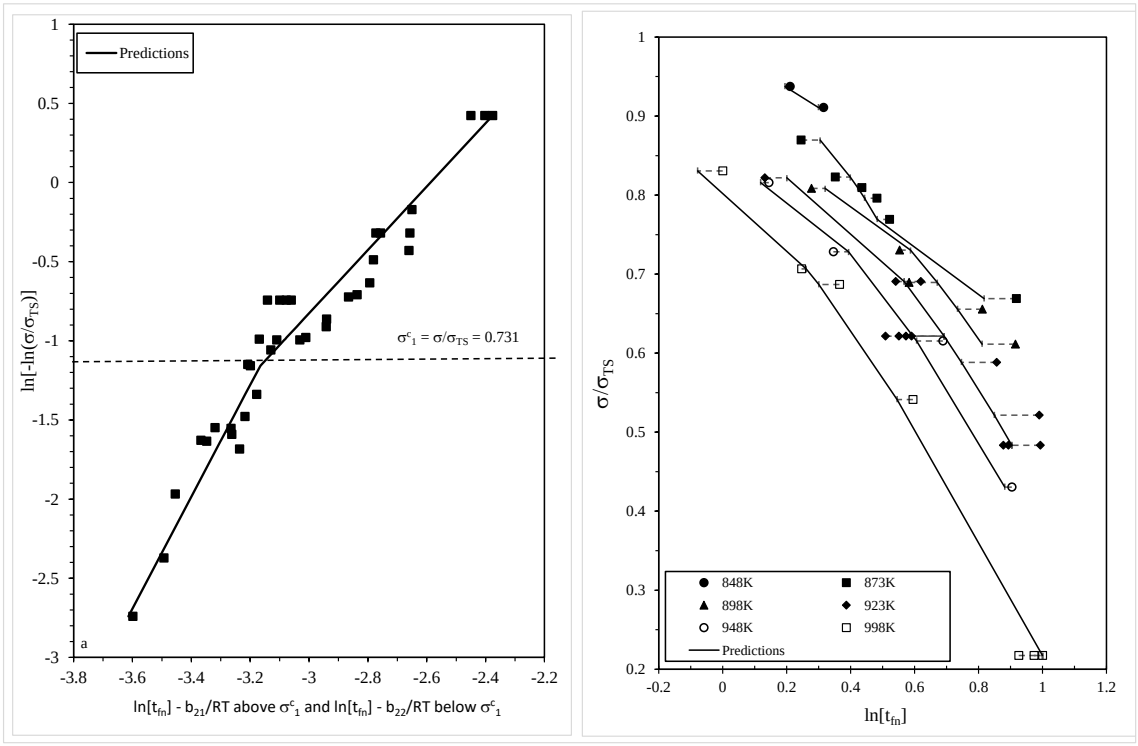

447

448 **Figure 2**. (a) Dependence of $\ln[t_{fn}] - b_{21}/RT$ above σ^c_1 and $\ln[t_{fn}] - b_{22}/RT$ below σ^c_1 on
449 $\ln[-\ln(\sigma/\sigma_{TS})]$ at all temperatures, (b) dependence of $\ln[t_{fn}]$ on (σ/σ_{TS}) with error bars
450 equal to the % prediction error/100.

451

452 The creep behaviour of Nickel based super alloys has been shown to be dependent
453 on applied condition with two distinct regions corresponding to stresses above and below
454 σ_Y (the yield stress) [29,13] – hence the observed kink point in Figure 2(a). This change
455 in creep behaviour is due to differing mechanisms of creep at different applied conditions.
456 Whittaker *et. al.* [29] highlighted the dominance of diffusive climb at stresses below σ_Y
457 (for Waspaloy) with dislocation-dislocation interaction in the form of forest hardening
458 limiting creep rates at higher stresses. Birosca *et. al.* [30] showed that geometrically
459 necessary dislocation (GND) densities are higher at the grain boundaries in Waspaloy
460 samples crept below σ_Y, where as GND densities were more uniformly spread through
461 grains in samples crept above σ_Y.

Figures 3(a,b) below contains Keyence images of two fine grained RR1000 RLH0569 creep specimens, giving examples of fracture surfaces expected at 660 MPa and 973K (Figure 3(a)), and 900MPa and 923K (Figure 3(b)). In both Figures 3(a,b) necking is observed with larger amounts seen in the latter. This necking is indictive of ductile failures, with necking increasing with increased stress.

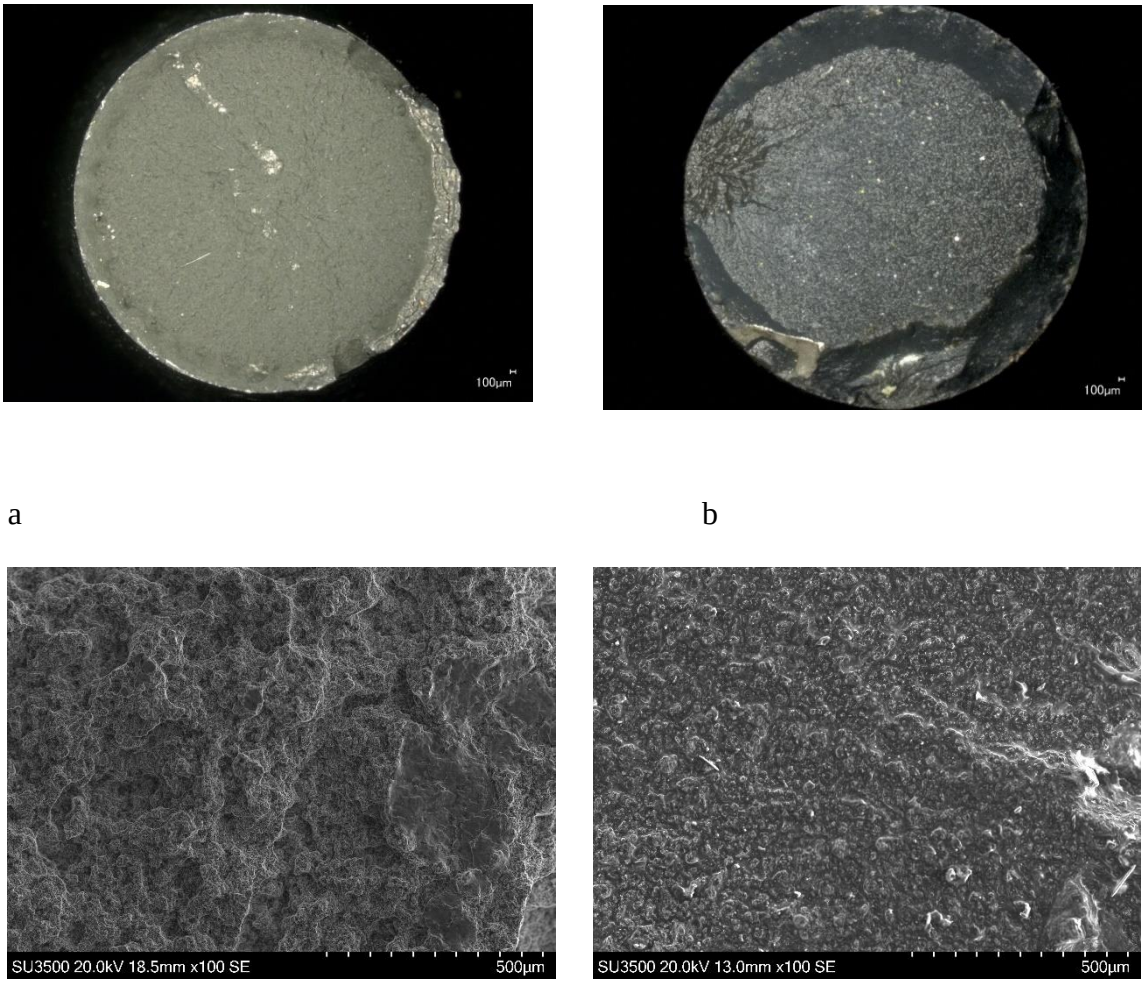

a b

c d

Figure 3. (a,c) Keyence images of fine grained RR1000 at 660 MPa and 973K, (b,d) at 900MPa

Figure 3. (a,c) Keyence images of fine grained RR1000 at 660 MPa and 973K, (b,d) at 900MPa and 923K.

In both Figures 3(c,d) a dull fibrous appearance can be observed, which again is representative of a ductile failure. Coalescence of micro voids (ductile dimples) is clearly visible on the surface of Figure 3(a), where as the micrograph of Figure 3(b) the micro voids appears to be more trans-granular in nature.

Table 2b summarises the ability of this Wilshire model to predict the actual (as in non-normalised) failure times. When the percentage errors shown by the length of the error bars in Figure 1(b) are squared and then averaged, the Wilshire model predicts with a 43.89% MPSE or with a root mean percentage squared error of 66.25%. This is put into further context by noting that Theil's U is 0.03, which is scaled to be within the range of 0 to 1- with zero corresponding to a model that produced perfect predictions. What is important to realise is that this average percentage error produced by the Wilshire model is all random (as $U^M = U^R = 0$) in nature suggesting the model is not mis-specified in any way, and that this mean percentage error reflects the natural variation present in measuring the times to failure from experimental creep curves (and so it is unlikely that this magnitude or error can be further reduced through use of any other creep model).

Table 2b. Summary of the predictive accuracy of equation [2d] using the parameter estimates shown in Table 2a.

The times to various strains

Using the method of estimation described above, Table 3a shows the parameter estimates of equation [3d] using as an example a normalised strain of $\varepsilon_n = 0.1$.

Table 3a. Least squares estimates of the parameters of equation [3d] when $\varepsilon_n = 0.1$.

The values for d_{21} and d_{22} are not shown in Table 3a. Instead, the activation energies that these parameter values imply are shown instead. It is not possible to show both these quantities as it would then be possible to rescale the normalised failure times to the true failure times values (within the margins of the experimental scatter). It is felt by the authors that the values for the activation energies are more informative than the values for d_{21} and d_{22}.

Parameter d_4 in equation [3e] produced a p-value of 5.38% meaning that the activation energies (Q_c^*) at a normalised strain of 0.1 above and below the normalised stress break point of 0.731 ($= \sigma_1^c$) are significantly different from one another at a significance level of 10%. The p-value associated with d_3 in equation [3e] is 1.523% suggesting that the values for z above and below the normalised stress of 0.731 are significantly different from each other at the 5% significance level. The coefficient of determination, R^2, shows that the model is capable of explaining 80.45% of the variation observed in the logarithm of normalised times to normalised strains of 0.1.

This Wilshire model visualised in Figure 4 where on the horizontal axis the normalised times to a normalised strain of 0.1 are temperature compensated. The performance of the Wilshire equation is seen by the suitability of the best fit line that is kinked at the break point defined by a normalised stress of 0.731. The predictions shown by the solid lines give a good fit to the actual times to normalised strains of 0.1. Equally good fits were obtained at other normalised strains.

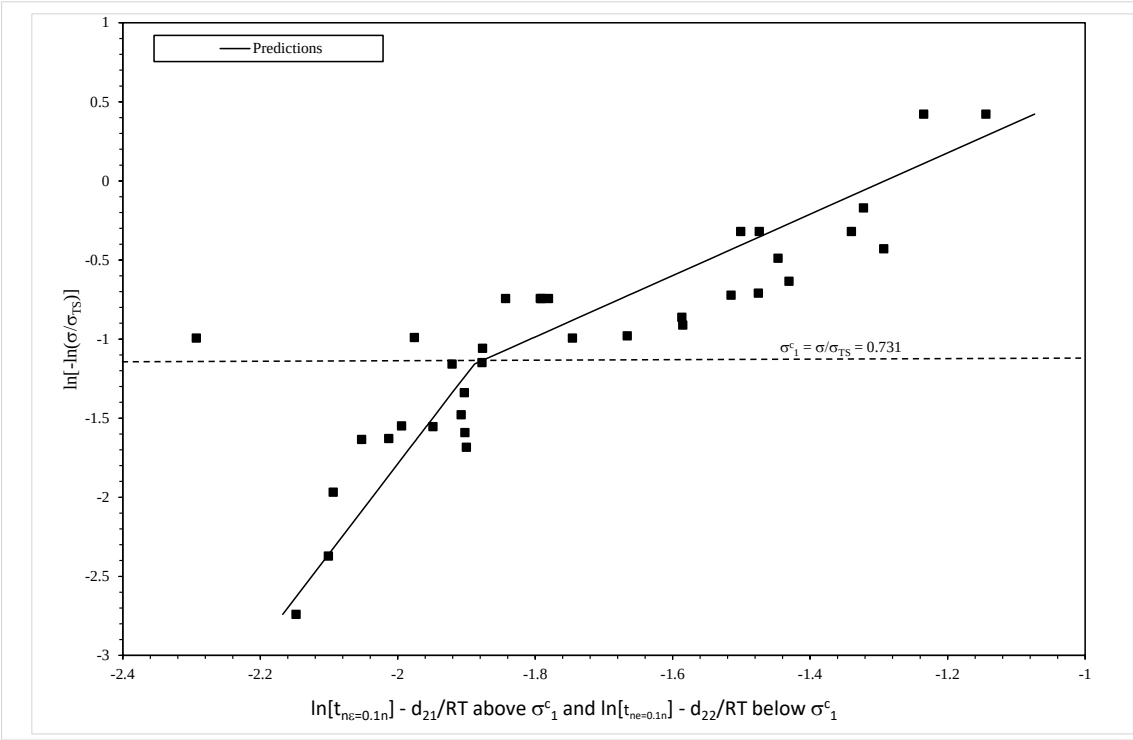

Figure 4. Dependence of $\ln[t_{n\varepsilon=0.1n} - d_{21}/RT]$ and $\ln[t_{n\varepsilon=0.1n} - d_{22}/RT]$ on $\ln[-\ln(\sigma/\sigma_{TS})]$ at all temperatures.

Table 3b summarises the ability of this Wilshire model to predict the actual (as in non-normalised) times to various strains. The Wilshire model predicts with a 205.1% MPSE or with a root mean percentage squared error of 143.2%. This is put into further context by noting that Theil's U is 0.19, which is scaled to be within the range of 0 to 1- with zero corresponding to a model that produced perfect predictions. What is important to realise is that this average percentage error produced by the Wilshire model is all random in nature (as $U^D = 1$) suggesting the model is not mis-specified in any way and that this mean percentage error reflects the natural variation present in measuring the times to stated normalised strains from experimental creep curves (and so it is unlikely that this magnitude or error can be further reduced through use of any other creep model).

Table 3b. Summary of the predictive accuracy of equations [3d] using the parameter estimates shown in Table 3a.

Figure 5 summarise the results from estimating the parameters of equation [3d] at all other normalised strains – from 0 to 1 in increments of 0.01. It can be seen that well defined relationships exists between the Wilshire parameters and the normalised strain. In Figure 5(a) it can be seen that d_{0j} decreases in a non-linear fashion with the normalised strain but this functional relationship is slightly different above and below the break point of σ^*_c. Unsurprisingly this is then reflected in different parameter estimates of equations [4b] as shown in Table 4. These parameter estimates produce the predicted curves (solid curves) shown in Figure 5(a) and as can be seen, the ANN produces a very good fit. Also notice that the d_{0j} obtained at each strain converge on the b_{0j} values of the failure time equation given by equation [2d] as the normalised strain tends to 1. In Figure 5(b), a positive but non-linearr relation to the normalised strain exists for d_{1j} above σ^c_1, but below σ^c_1 there is vary little variation in the parameter with respect to the normalised stress. Again, this is then reflected in different estimates of the parameters in equation [4a] as shown in Table 4. These parameter estimates produce the predicted curves (solid curves) shown in Figure 5(b) and as can be seen the ANN again produces a very good fit. Also notice that the d_{1j} obtained at each strain converge on the $1/u_j$ of the failure time equation given by equation [2a] as the normalised strain tends to 1. In Figure 5(c) the values of Q^*_c (in $Jmol^{-1}$), are the activation energies associated with differing strains, and they appear to depend strongly on the normalised strain but in a fashion that is very similar above and below the break point of $\sigma^1_{c.}$ The difference in the Q^*_c values each side of this break point diminishes as the normalised strain decreases, but again the Q^*_c values obtained at each strain converge on the Q^*_c values of the failure time equation given by equation [2d] as the normalised strain tends to 1. The shape of the curves in Figure 5(c)

564 are consistent with the work of Estrin and Mecking [23] with Q^*_c being viewed as the
565 activation energy for steady state or minimum creep.

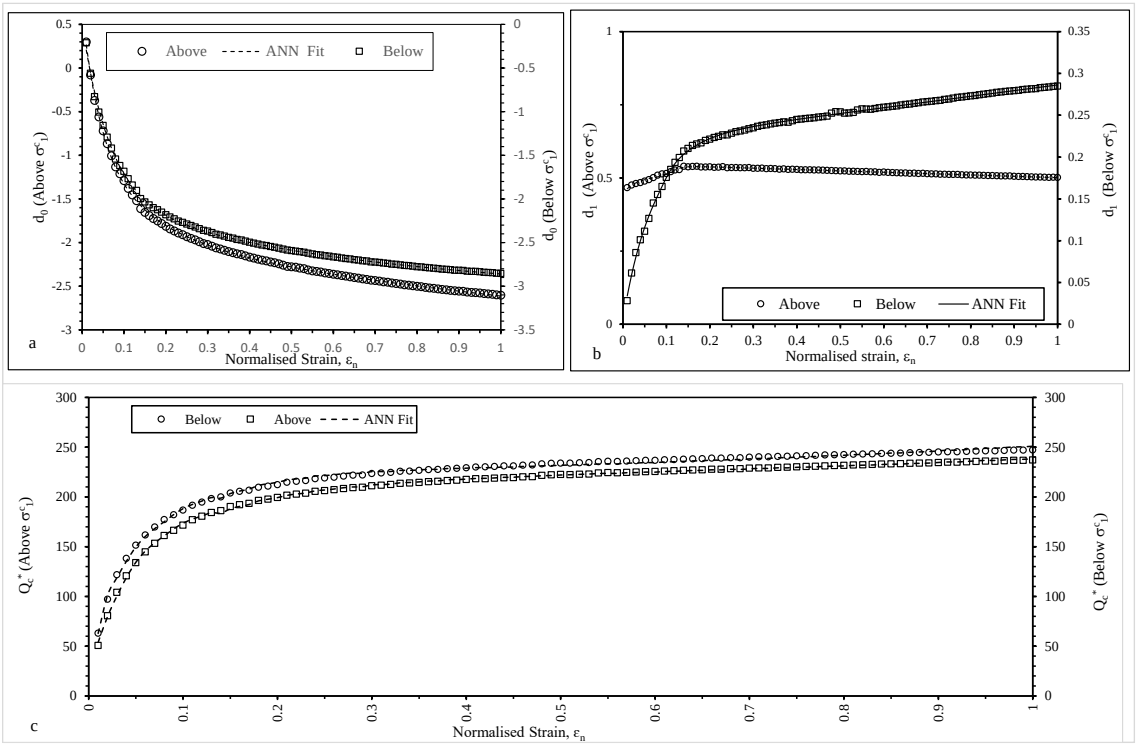

566

567 **Figure 5.** Variations of the Wilshire parameters with normalised strain: (a) d_0, (b) d_1, (c)
568 Q^*_{cj} (Jmol^{-1}).

569
570 **Table 4.** Parameter estimates of equations [4a,b,c].

571

572 ***Individual creep curves***

573 Table 3b only shows the performance of the Wilshire equation at a normalised
574 strain of 0.1, but to assess its full performance this analysis is repeated for all normalised
575 strains – in increments of 0.01. Table 5 summarises the results of such an analysis. This
576 involved the following steps: 1. Insert the parameters estimates shown in Table 4 into
577 equations [4] to predict the parameters d_{0j}, d_{1j} and Q^*_{cj} at all normalised strains ε_n. 2. Insert
578 these predicted values for the parameters d_{0j}, d_{1j} and Q^*_{cj}, together with all the stress and
579 temperatures in the experimental data set into equation [3d] to predict the (normalised

log) time taken to reach all these strains at all these stresses and temperatures (noting that the parameter d_{2j} in equation [3d] is given by $Q_{cj}^{*}/\{\ln[t_{n\varepsilon n}]_{max} - \ln[t_{n\varepsilon n}]_{min}\}$). 3. Compare the predicted times to all the strains to the experimentally measured ones and then apply equations [7] and equations [8] to assess how close the predicted and experimental values are. The statistics in equations [7b,8e,8f] can be obtained by calculating these statistics over all test conditions at a stated normalised strain, and then repeating this calculation for all strains and then averaging the 100 (100 increments of the normalised strains) values for MPSE, U^M, U^R, U^D and U. These values are shown in the first column of Table 5. This is tantamount to assessing the accuracy of the technique in predicting the same point on all the creep curves (that point being defined by a normalised strain value). Alternatively, the statistics in equations [7b,8e,8f] can be calculated by calculating these statistics over all the normalised strains at a stated test condition, and then repeating this calculation for all the test conditions and then averaging the 37 (37 test conditions) values for MPSE, U^M, U^R, U^D and U. These values are shown in the second column of Table 5. This is tantamount to assessing the accuracy of the technique in predicting complete creep curves.

Table 5. Summary of the predictive accuracy of equation [3d] using the parameter estimates shown in Table 4 for equations [4] and all the experimental stress and temperature test conditions.

From the first column of Table 5 it can be seen that the Wilshire-ANN approach is capable of predicting the time taken to reach a specified strain at a given test condition very accurately – the RMPSE is only around 10%. Furthermore, 98% of this prediction error is random in nature. Consequently, there is no tendency to continually over predict this time at some test conditions or under predict at others. This is true not matter what strain (i.e. point on the creep curve) is chosen. This result is just a reflection of the random

scatter of the date points around the best fit segmented line in Figure 4 – when considering the time taken to reach 0.2 normalised strain.

The second column of Table 5 reveals that the Wilshire-ANN approach does less well at predicting the shape of a whole creep curve at a stated test condition. The Wilshire time to strain equation predicts the 37 normalised creep curves (associated with the 37 test conditions) with a RMPSE of 80.93%. This is put into further context by noting that Theil's U is 0.12, which is scaled to be within the range of 0 to 1, with zero corresponding to a model that produced perfect predictions. Whilst this error is reasonable given the stochastic nature of creep, only 3% of these prediction errors are random. This systematic nature of the prediction errors is a reflection of the failure time date points being dispersed around the best fit segmented line in Figure 2a, rather than on it. So for any particular test condition, the actual failure time differs from what is predicted by the Wilshire equation for t_f. This will cause the Wilshire-ANN creep curve prediction to then be either consistently below or above the actual curve at all strains at a particular test condition. Despite the systematic error, the shape of the predicted curve can still resemble the experimental one.

This systematic prediction error is not as serious as it sounds, in that the Wilshire-ANN creep curve prediction can be visualised as the mean creep curve that would be obtained by doing many repeat creep tests at the same condition. Thus the experimental creep curve obtained at a particular test condition in the date set used here, is really a measure of some percentile of the distribution of creep curves at that condition and not the true creep curve. In this visualisation, there is no reason to expect the average creep curve prediction to correspond exactly to the measured curve.

These points can be elaborated on with reference to Figures 6, 7 and 8. Figure 6 plots the RMPSE associated with each of the 37 test conditions making up the experimental data set. As seen in Table 5, the average error over all test conditions is 80.93%, but as seen in Figure 6 there are big disparities across all the experimental test conditions. For example, take the test condition 848K and 1370 MPa which is highlighted in Figure 6. The RMPSE associated with this predicted creep curve is just 11%, and as can be seen from Figure 7a, the predicted creep curve follows closely the shape of the experimental creep curve. Similarly good predictions are also obtained for the creep curves at the other three test conditions illustrated in Figure 7.

At the other end of the spectrum, take the test condition 923K and 900 MPa which is also highlighted in Figure 6. The RMPSE associated with this predicted creep curve is just under 107% and as can be seen from Figure 8c, the predicted creep curve does not follow closely the shape of the experimental creep curve. More specifically, the Wilshire-ANN approach appear to predict the primary stage of creep well, but not the nature of the tertiary stage, Similarly mediocre predictions are also obtained for the creep curves at the other three test conditions illustrated in Figure 8. It can also be seen in Figure 6, that creep curve predict tends to be better at higher stresses. There is also a tendency for times to all 100 normalised strains to be more accurately predicted at the highest and the lowest recorded temperature irrespective of the stress.

650 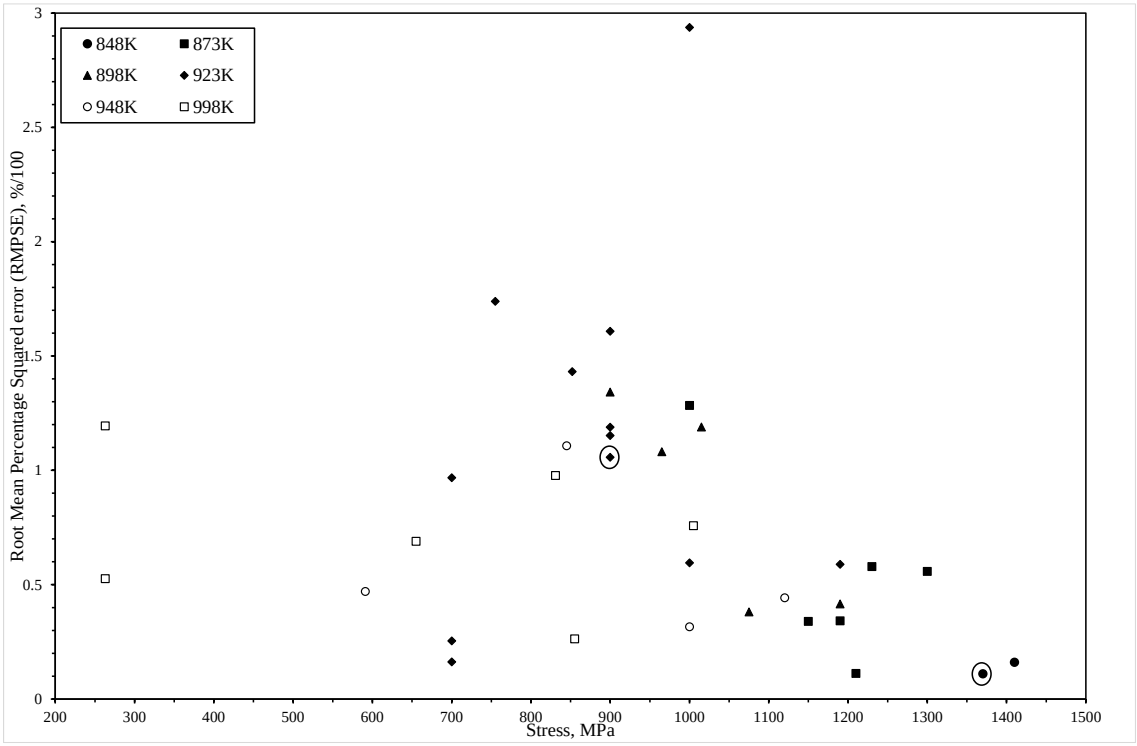

651 **Figure 6.** The predictive accuracy of the time to strain equation at different test
652 conditions as measured by the RMSPE.

653

654 Finally, Figure 7 & Figure 8 plot the experimentally obtained creep curves,
655 together with the corresponding predictions of these curves obtained using the Wilshire
656 model (modified with an ANN) at eight illustrative but different test conditions. The
657 vertical axis has the normalised strain, whilst on the horizontal axis time is scaled by the
658 failure time to protect the units of the data for commercial reasons. At all four test
659 conditions shown in Figure 7, the model gives a good prediction of the shape of the
660 experimental creep curves. Even for a RMPSE of around 25%, it can be seen that the
661 predicted curve is also quite close to the experimental one (as at 998K and 855 MPa).
662 This is important when it comes to using these equations to numerically model the small
663 punch test. The small differences between the predicted and actual creep curves seen in
664 Fig. 7 reflects of course the relative small errors made in predicting the times to failure at
665 these test conditions.

Figure 8 show the actual and predicted creep curves for those test conditions leading to moderate to higher RMPSE values. In Figures 8a,b, the RMPSE are in the 60 and 100% ranges and it can be seen that whilst the creep curves diverge, the shapes of the actual and predicted curves are quite similar – with little or no tertiary creep. for the selected test conditions shown there. Figures 8c,d corresponds to test conditions where the RMSPSE is around or above 100% and here the predicted creep curve shapes are also very different to that seen in the experimental curves.

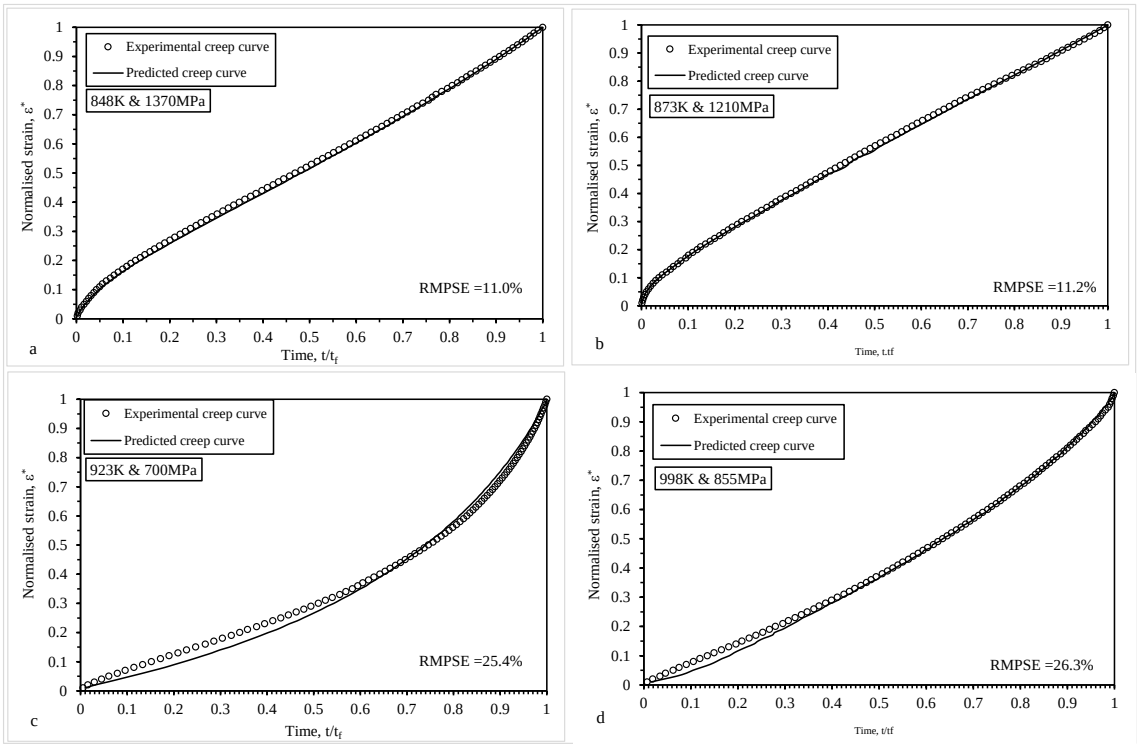

Figure 7. Experimental and predicted creep curves at four different illustrative test conditions: (a) 848K and 1370 MPa,(b) 898K and 1190 MPa, (c) 923K and 700 MPa, (d) 998K and 855 MPa.

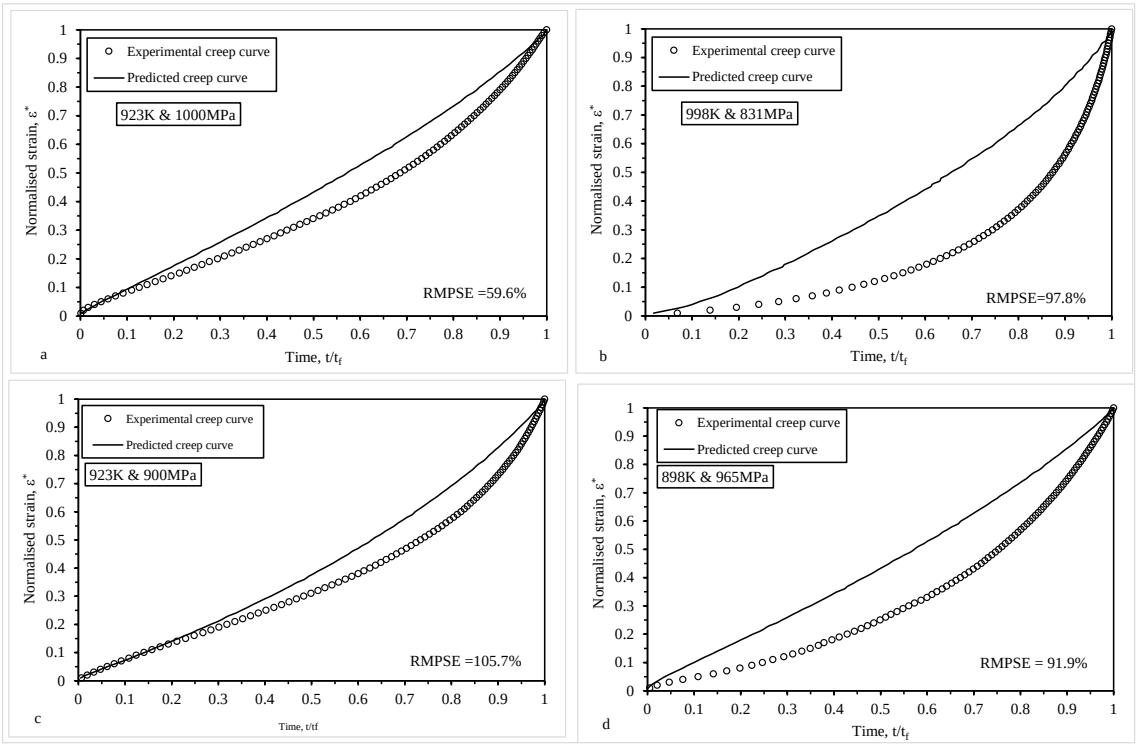

Figure 8. Experimental and predicted creep curves at four different illustrative test conditions: (a) 923K and 1000 MPa,(b) 998K and 831 MPa, (c) 923K and 900 MPa, (d) 898K and 965MPa.

Conclusion

This paper introduced an artificial neural network (ANN) methodology for extending the Wilshire Equation related to times to specified strains so that complete creep curves can be predicted at any test conditions (including operating conditions) using just accelerated test data. The paper also presented various statistics for the evaluation of predictions made by the this modified Wilshire model. These statistics also provide a suitable way of comparing different creep prediction models as they are scaled values and so should prove useful in future research on creep prediction. When these techniques and predictions were applied to RR1000 the following conclusions could be drawn:

1. A small but statistically significant change occurred in the activation energy for RR1000 at a normalised stress of 0.731.

2. Using the Wilshire time to strain equation expressed in normalised strain space, it was possible to measure the activation energy at various different strains and the results support the work of Estrin and Mecking [23] who proposed that the activation energy would be dependent on strain in the way seen in this paper.

3. The Wilshire equations for failure times produce very good predictions, with U values very close to zero and with root mean squared percentage errors of 66.25%.

4. The parameters of the Wilshire time to strain equation have a well defined and systematic relationship with the normalised strain and these functional relationships are extremely well modelled using a simple artificial neural network (ANN). Because the parameters tend in value to those of the Wilshire time to failure equation as the normalised strain tends to 1, the predicted creep curves are well behaved in that they do not "curve back on themselves" at high strains.

5. The model works well at predicting creep curves with a U of 0.12 over all strains and test conditions. When the ANN is combined with the Wilshire equation for times to strains, the shape of the creep curve is well predicted at all temperatures, when the stress is 1000 MPa or more. Where there is a scale discrepancy at other test conditions the technique predicts the shape of the creep curve well. That said, for most test conditions present in the experimental data set used for this paper, the predicted creep curves were in very close agreement with the experimental curves with a root mean squared percentage errors less than 80.93%.

722 The ANN equations estimated in this paper can in future research be built into
723 finite element code for the small punch test where they can be used to model times to
724 incremental strains and therefore to correlate small punch test data with uniaxial results
725 for RR1000.
726
727 **Acknowledgements**: The authors would like to thank Rolls-Royce for their financial
728 support and technical involvement in this research, and in supplying the experimental
729 data and test material used within this paper. We would also like to thank EPSRC for their
730 funding support – Industrial Case Award EP/R512102/1.
731 .
732

References

[1] Abdallah Z, Perkins K, Williams S. Advances in the Wilshire extrapolation technique-Full creep curve representation for the aerospace alloy Titanium 834. M*aterials Science and Engineering A* [Internet], 2012;550:176–182. Available from: http://dx.doi.org/10.1016/j.msea.2012.04.054.

[2] Strategic Research Agenda. Materials UK Energy Review: Report 1, Energy Materials. 2007.

[3] Wilshire B, Battenbough AJ. Creep and creep fracture of polycrystalline copper. *Materials Science and Engineering A*, 2007; 443:156-166.

[4] Whittaker MT, Harrison WJ. Evolution of Wilshire equations for creep life prediction. Mater. High Temp. 2014;31:233–238.

[5] Wilshire B, Scharning PJ. Prediction of long term creep data for forged 1Cr-1Mo-0.25V steel. *Materials Science and Technology*, 2008;24(1):1-9.

[6]. Wilshire B, Whittaker M. Long term creep life prediction for Grade 22 (2·25Cr-1Mo) steels. *Materials Science and Technology*, 2011; 27(**3**): 642-647.

[7] Evans M. Incorporating specific batch characteristics such as chemistry, heat treatment, hardness and grain size into the Wilshire equations for safe life prediction in high temperature applications: An application to 12Cr stainless steel bars for turbine blades. *Applied Mathematical Modelling*, 2016; 40(**23-24**): 10342-10359.

[8] Wilshire B, Scharning PJ. A new methodology for analysis of creep and creep fracture data for 9–12% chromium steels. *International Materials Reviews*, 2008; 53(**2**):91-104.

[9] Whittaker MT, Evans M and Wilshire B. Long-term creep data prediction for type 316H stainless steel. *Materials Science and Engineering A*, 2012; 552:145-150.

[10] Wilshire B, Scharning PJ. Extrapolation of creep life data for 1Cr-0.5Mo Steel. *Int. J. Press. Vessel. Pip*., 2008; 85: 739–743.

[11] Whittaker MT, Harrison WJ, Lancaster RJ, Williams S. An analysis of modern creep lifing methodologies in the Titanium alloy Ti6-4. *Mater. Sci. Eng. A*, 2013; 577: 114–119.

[12] Whittaker MT, Harrison WJ, Williams S. Recent Advances in Creep Modelling of the Nickel Base Superalloy, Alloy 720Li. *Materials*. 2013; 6: 1118–1137.

[13] Evans M, Williams TA. Assessing the capability of the Wilshire equations in predicting uniaxial creep curves: An Application to Waspaloy. *Int. J. Press. Vessel. Pip*., 2019; 172:. 153–165.

[14] Mitchell RJ, Lemsky JA, Ramanathan R, Li HY, Perkins KM, Connor LD. Process Development and Microstructure and Mechanical Property Evaluation of a Dual Microstructure Heat Treated Advanced Nickel Disc Alloy. In: Reed RC, editor. Superalloys 2008: Edited by Roger C. Reed ... [et al.]. Warrendale: Tms-Minerals; 2008: 347–356 .

[15] Mitchell RJ, Hardy MC, Preuss M, Tin, S. Development of γ′ morphology in P/M rotor disc alloys during heat treatment. In *Proc. Int. Symp. Superalloys*, 2004: 361–70.

[16**]** Reed RC. *The Superalloys: Fundamentals and Applications*. Cambridge: Cambridge University Press; 2006.

[17] Chong Y, Liu Z, Godfrey A, Liu W, Weng Y. The Application of Grain Boundary Engineering to a Nickel Base Superalloy for 973 K (700 °C) USC Power Plants. *Metall. Mater. Trans E*. 2014; 1(**1**): 58–66.

[18] Abdallaha, Z, Perkins, K and Williams, S. Advances in the Wilshire extrapolation technique—Full creep curve representation for the aerospace alloy Titanium 834. *Materials Science and Engineering: A*, 2012; 550(**30**): 176-182.

782 [19 Harrison, W, Whittaker MT, Williams, S. Recent Advances in Creep Modelling of
783 the Nickel Base Superalloy, Alloy 720Li. *Materials*, 2013; 6: 1118–1137.

784 [20] Gray, V and Whittaker, MT. Development and Assessment of a New Empirical
785 Model for Predicting Full Creep Curves. *Materials*, 2015; 8: 4582-4592.

786 [21] Martin, VC, Hurn, S, Harris, D. *Econometric Modelling with Time Series:*
787 *Specification, Estimation and Testing*, Cambridge University Press, Cambridge, 2013.

788 [22] Davies RG. On the activation energy of high temperature creep. *Acta Metallurgica*,
789 1961; 9: 1035-1036.

790 [23] Estrin, Y and Mecking, H. A unified phenomenological description of work
791 hardening and creep based on one-parameter models. *Acta Metallurgica*, 1984;
792 32(**1**): 57-70

793 [24] Akaike, H. On Entropy Maximisation Principle. In Krishniah, PR (ed.),
794 *Applications of Statistics*. Amsterdam; North Holland: 1977.

795 [25] Monkman FC, Grant NJ. An empirical relationship between rupture life and
796 minimum creep rate in creep-rupture tests. *Proc. ASTM.* 1956; 56: 593–620.

797 [26] Dunand, DC, Han, BQ and Jansen, AM. Monkman-Grant analysis of creep
798 fracture in dispersion-strengthened and particulate-reinforced aluminium. *Metallurgical*
799 *and Materials Transactions A*, 1999; 30(**13**): 829-838.

800 [27] Holden, K, Peel, DA and Thompson, JL. *Economic Forecasting: An Introduction*.
801 Cambridge University Press; Cambridge: 1990.

802 [28] Theil, H. *Applied Economic Forecasts*. Amsterdam; North Holland: 1966.

803 [29] M. Whittaker, W. Harrison, C. Deen, C. Rae, S. Williams: Creep deformation by
804 dislocation movement in Waspaloy, Materials (Basel), 10, 2017.

[30] S. Birosca, G. Liu, R. Ding, J. Jiang, T. Simm, C. Deen, M. Whittaker: The dislocation behaviour and GND development in a Nickel based superalloy during creep, Int. J. Plast., 118, 2019, pp. 252–268.